1 **Hydrogen peroxide in the marine boundary layer over the southern Atlantic**

2 **during the OOMPH cruise in March 2007**

3 Horst Fischer[1], Andrea Pozzer[1], Torsten Schmitt[1], Patrick Jöckel[2], Tim Klippel[1], Domenico

4 Taraborrelli[1], and J. Lelieveld[1]

5 [1]Max Planck Institute for Chemistry, Department of Atmospheric Chemistry, Mainz, Germany

6 [2]Deutsches Zentrum für Luft- und Raumfahrt (DLR), Institut für Physik der Atmosphäre,

7 Oberpfaffenhofen, Germany

8 Correspondence to: Horst Fischer (horst.fischer@mpic.de)

9

10 **Abstract**

11 In the OOMPH (Ocean Organics Modifying Particles in both Hemispheres) project a ship

12 measurement cruise took place in the late austral summer from 1st to 23rd March, 2007. The

13 French research vessel Marion Dufresne sailed from Punta Arenas, Chile (70.85°W, 53.12°S) to

14 La Reunion island (55.36°E, 21.06°S) across the southern Atlantic Ocean. In-situ measurements

15 of hydrogen peroxide, methylhydroperoxide and ozone were performed and are compared to

16 simulations with the atmospheric chemistry global circulation model EMAC. The model

17 generally reproduces the measured trace gas levels, but underestimates hydrogen peroxide mixing

18 ratios at high wind speeds, indicating too strong dry deposition to the ocean surface. An

19 interesting feature during the cruise is a strong increase of hydrogen peroxide,

20 methylhydroperoxide and ozone shortly after midnight off the west coast of Africa due to an

21 increase in the boundary layer height, leading to downward transport from the free troposphere,

22 which is realistically reproduced by the model.

23

24 **1 Introduction**

25 The oxidizing power of the lower atmosphere in the gas phase is defined by the concentrations of

26 the hydroxyl radical (OH), ozone (O_3), the nitrate radical (NO_3), halogen radicals (e.g. ClO, BrO,

27 IO) and hydrogen peroxide (H_2O_2), an important oxidizer in the liquid phase (Thompson, 1992).

28 The dominant oxidizing agent is OH, whose primary source is the photolysis of O_3 and

29 subsequent reaction of the formed O^1D-atom with water vapor (Levy, 1971). The major sinks of

30 OH are reactions with carbon monoxide (CO), methane (CH_4), and volatile organic compounds

31   (VOC) yielding peroxy radicals (HO_2 and RO_2). The fate of these peroxy radicals strongly

32   depends on the concentrations of nitrogen oxides (NOx, NO plus NO_2). In semi-polluted and

33   polluted regions with NOx levels in excess of several tens of pptv, the peroxy radicals

34   predominantly react with NO, yielding NO_2 and recycling OH. In these environments the

35   subsequent photolysis of NO_2 yields ozone, with NOx acting as a catalyst. In low NOx

36   environments, such as the marine boundary layer, the peroxy radicals undergo self-reactions

37   ($HO_2 + HO_2$ and $RO_2 + HO_2$) yielding H_2O_2 and organic peroxides (e.g. CH_3OOH from methane

38   oxidation), and also destroying ozone ($HO_2 + O_3$ and $OH + O_3$). The peroxides serve as reservoir

39   species for the HOx (OH plus HO_2) radicals, which can be recycled by photolysis or reaction

40   with OH. Hydrogen peroxide is also an important oxidizing agent in the liquid phase, notably of

41   sulfur dioxide. Since many peroxides are water soluble, physical removal processes (deposition

42   to surfaces and washout in rain events) strongly influence the oxidizing power of the lower

43   atmosphere.

44   In the marine boundary layer at low NOx concentrations the concentrations of H_2O_2, ROOH and

45   O_3 are strongly coupled, since their formation and destruction compete for the HO_x radicals. In

46   order to model oxidation processes in this environment, formation and destruction of peroxides

47   have to be accurately described, including the physical removal processes.

48   Previous measurements of peroxides (H_2O_2 and ROOH) in the marine boundary layer in the

49   1980s and 1990s have been summarized in the review article by Lee et al. (2000). Since this

50   review additional observations in the marine boundary layer have been reported in the literature

51   (Junkermann and Stockwell, 1999; Weller et al., 2000; Kieber et al., 2001; O'Sullivan et al.,

52   2004; Chang et al., 2004; Stickler et al., 2007). These observations indicate highest mixing ratios

53   (> 500 pptv) of H_2O_2 in the tropics (Slemr and Tremmel, 1994; Heikes et al., 1996; O'Sullivan et

54   al., 1999; Junkermann and Stockwell, 1999; Weller et al., 2000; O'Sullivan et al., 2004) and

55   decreasing concentrations toward higher latitudes in both hemispheres, reaching 200 – 300 pptv

56   south of 40° in the southern hemisphere (Slemr and Tremmel, 1994; O'Sullivan et al., 1999;

57   Junkermann and Stockwell, 1999; Weller et al., 2000; O'Sullivan et al., 2004). In general mixing

58   ratios are about a factor of two higher in the northern hemisphere than at corresponding latitudes

59   in the south (O'Sullivan et al., 1999). A significant dissimilarity between the different ocean

60   basins has not been observed, while higher H_2O_2 mixing ratios have been observed in continental

61   outflow (e.g. Heikes et al., 1996).

62   The mixing ratios of the most abundant organic peroxide CH_3OOH show similar behavior as

63   H_2O_2 in the marine boundary layer, with highest levels in the tropics and decreasing towards the

64   poles. Also the absolute mixing ratios are comparable, yielding H_2O_2/CH_3OOH ratios close to 1

65   in air masses not affected by recent rainout (Lee et al., 2000).

66   Here we describe in-situ ship-based observations of O_3, H_2O_2 and a proxy for CH_3OOH in the

67   marine boundary layer of the southern Atlantic Ocean in the austral late summer of 2007. These

68   measurements are compared to the atmospheric chemistry global circulation model EMAC

69   (Jöckel et al., 2006, Jöckel et al., 2010). Section 2 describes the methods (measurement principles

70   and model) used, while the observations and model comparisons are described and discussed in

71   section 3. The final section summarizes the findings of this study.

72

73   **2 Methods**

74

75   **2.1 OOMPH cruise MD160**

76   As part of the OOMPH (Ocean Organics Modifying Particles in both Hemispheres) project a

77   measurement cruise took place in the late austral summer from 1st to 23rd March, 2007. The

78   French research vessel Marion Dufresne sailed from Punta Arenas, Chile (70.85°W, 53.12°S) to

79   La Reunion island (55.36°E, 21.06°S) crossing the southern Atlantic between the east coast of

80   South America to the southern Indian Ocean east of South Africa between 20°W, 60°S and 35°E,

81   35°S (Figure 1). During the first part of the cruise at high southern latitudes, cold air was

82   encountered from the Antarctic continent. During this part of the cruise, cloud cover was

83   extensive. Further north, temperatures increased together with solar radiation intensity and

84   photolysis frequencies. The wind was generally from the west, with wind speeds varying between

85   calm conditions and gale force winds up to 33 ms^{-1}. The average wind varied between more than

86   10 ms^{-1} during the first part and 8 ms^{-1} during the second part of the campaign (Figure 2). Details

87   of the cruise can be found in Williams et al. (2010) and Hosaynali Beygi et al. (2011).

88

89   **2.2 Trace gas measurements**

90   Data used in this study were obtained by two in-situ instruments mounted in a temperature

91   controlled container placed on the foredeck of the ship (see Fig. 3 in Hosaynali Beygi et al.,

92   2011). Air was sampled from the top of an atmospheric mast (10 m above the deck, 20-25 m

93   above the sea surface) through 17.1 m ½" Teflon tubes, shielded from sunlight by a black cover.

94   The inlet was designed as a bypass with a total flow of 24 slm (retention time 3.4 s) sustained by

95   a membrane pump. From the bypass inlet small flows were directed to the in-situ instruments

96   inside the container via short ¼" Teflon lines.

97   Hydrogen peroxide (H_2O_2) was measured with a commercial analyzer (AL2001 CA, Aero Laser,

98   Garmisch Partenkirchen, Germany) based on wet chemical dual enzyme detection scheme

99   described by Lazarus et al. (1985, 1986). Gaseous peroxides are sampled in a buffered (potassium

100   hydrogen phthalate/NaOH) sampling solution (pH 5.8) in a glass stripping coil at a flow of 3 slm.

101   The sampling efficiency for H_2O_2 was determined several times in the field and was always

102   higher than 0.8. After passing the sampling coil the degassed liquid peroxide solution is divided

103   into two channels and subsequently reacts with p-hydroxyphenyl acetic acid (POPHA) and

104   horseradish peroxidase. The reaction with hydrogen peroxide, organic hydroperoxides and

105   organic peroxides yields a fluorescent dye (6,6'-dihydroxy-3,3'-biphenyldiacetic acid) in

106   stoichiometric quantities that is subsequently detected via fluorescence spectroscopy at 400-420

107   nm after excitation at 326 nm with a Cd ray lamp in a detection cell. Since the detection scheme

108   is unspecific, the H_2O_2 concentration is determined from the difference of the two channels, with

109   channel A measuring all peroxides (ROOH), while channel B measures ROOH – H_2O_2 after

110   selective destruction of H_2O_2 via addition of catalase (efficiency > 95% as determined in the

111   field) prior to the reaction with POPHA. Thus the difference between both channels provides the

112   H_2O_2 concentration, while channel B provides an unspecific measurement of all organic

113   hydroperoxides and organic peroxides. Nevertheless, assuming that methylhydroperoxide (MHP;

114   CH_3OOH) is the most abundant organic peroxide in the remote marine boundary layer, as shown

115   by previous measurements (e.g. Heikes et al., 1996), we obtain an upper limit assuming that

116   ROOH consists of MHP only. The organic peroxide data is subsequently corrected for the lower

117   sampling efficiency of CH_3OOH compared to H_2O_2. The time resolution (10–90%) of the

118   instrument is 30 sec.

119   The in-field calibration of the instrument involves regular zero gas measurements (scrubbed

120   ambient air after passage through cartridges filled with silica gel and hopcalite (Infiltec, Speyer,

121   Germany)), liquid calibrations (liquid H_2O_2 standard of 35.5 $\mu g l^{-1}$) and gas phase calibrations

122   with a H_2O_2 permeation tube (30% H_2O_2 in a glass flask temperature controlled to 40°C

123   providing a calibration gas concentration of 6.38 ppbv). The detection limit of the instrument was

124   determined from the 1σ variability of the in-field zero measurements performed every 2.5 h,

125 estimated at 25 pptv. The total uncertainty determined from the precision (1σ variability of 9 in-

126 field gas phase and liquid calibrations), the uncertainty of the standard, the inlet transmission and

127 an ozone interference correction was about 12-13 %. During the campaign the inlet transmission

128 was determined twice by adding the gas phase standard at the top of the inlet line. Comparison of

129 two calibrations directly in front of the analyzer yielded a transmission that decreased from 67%

130 at the beginning of the campaign to 57% towards the end. The instrument has also been used (in

131 combination with a constant pressure inlet) for airborne measurement of H_2O_2 in the free

132 troposphere over the rainforest in South America (Stickler et al., 2007) and over Europe (Klippel

133 et al., 2011).

134 A discussion of uncertainties of the MHP measurements can be based on extreme cases (all

135 ROOH is MHP vs. no MHP at all). The model analysis on ROx radicals presented in Hosaynali

136 Beygi et al. (2011) indicates that no other organic peroxy radicals other than CH_3O_2 are expected

137 in the very clean marine boundary layer, indicating that MHP dominates the ROOH signal of the

138 analyzer. A sampling efficiency of 60 % for MHP is a reasonable assumption. The efficiency

139 cannot be higher than that for H_2O_2 (95 %) and is unlikely smaller than 30 %, thus yielding an

140 uncertainty of ± 30 %. One should also mention that catalase reacts to some extend with MHP.

141 The commercial analyzer (AERO-Laser, Model AL 2001CA) that has been used is based on the

142 original design of Lazarus et al. (1986). As discussed in this paper, the effect of catalase

143 destruction on MHP is estimated to be about 3 %, an order of magnitude less than the uncertainty

144 due to the sampling issue discussed above.

145 The detection limit is determined from the reproducibility of the zero air measurements in both

146 channels of the analyzer and strictly applies to the H_2O_2 channel. A rough estimate for MHP can

147 be gained by multiplying with the sampling efficiency of 0.6, yielding a value of 40 pptv.

148 The instrument used to measure ozone (together with NO and NO_2) is a high resolution (1 s) and

149 highly sensitive 3-channel chemiluminescence detector (CLD, ECO-Physics CLD 790 SR,

150 Duernten, Switzerland). The instrument and its performance characteristics during this campaign

151 have been described in detail in a previous publication on the NOx/O_3 photostationary state by

152 Hosaynali Beygi et al. (2011). The total uncertainty for the O_3 channel was determined from the

153 2σ deviation of the in-field calibrations (ozone calibrator model TE49C, Thermo Instruments,

154 Germany) and the accuracy of the standard, estimated at 1% (Hosaynali Beygi et al., 2011).

155

156 **2.3 Atmospheric chemistry model EMAC**

157   Simulations of trace gas mixing ratios along the ship cruise were performed using the EMAC

158   (ECHAM/MESSy Atmospheric Chemistry) global circulation model (Jöckel et al., 2010). EMAC

159   uses the Modular Earth Submodel System (MESSy; Jöckel et al., 2005) to link multi-institutional

160   sub models describing atmospheric processes interacting with oceans, land and human influences.

161   For this study EMAC was applied in the T42L90MA-resolution ($2.8°$ x $2.8°$ resolution in latitude

162   and longitude, 90 vertical levels up to 0.01 hPa), using results from the lowest model level

163   (~30m) for comparison with measurements. The model was sampled (spatial bilinearly

164   interpolated) along the ship track at every time step (i.e. 12 minutes) using the SD4 submodel

165   (Jöckel et al., 2010), without any temporal interpolation. The meteorology was nudged to the

166   operational ECMWF analysis. Tropospheric gas-phase and heterogeneous chemistry was

167   calculated with the sub-model MECCA (Module Efficiently Calculating the Chemistry of the

168   Atmosphere; Sander et al., 2005), aqueous-phase chemistry in cloud droplets and wet scavenging

169   with the sub-model SCAV (Tost et al., 2006) and primary emissions and dry deposition of trace

170   gases and aerosols with the sub-models ONLEM, OFFLEM, TNUDGE and DRYDEP (Kerkweg

171   et al., 2006a and 2006b). Previous results of a model comparison with airborne H_2O_2

172   measurements in the free troposphere have been discussed in Klippel et al. (2011).

173

174   **3 Results and discussion**

175

176   **3.1 Data processing**

177   For the present analysis the original observations were averaged over 12 minute time intervals to

178   be coherent with the model output time stepping. The time scale used is UTC, thus leading to

179   deviations from solar noon of -80 min for the most westerly point ($20°W$) of the ship track to 140

180   min for the most easterly ($35°E$). Unfortunately due to the prevailing westerly winds the

181   instruments often measured air polluted by the ship exhausts, notably when the wind was from

182   the sector between $55°$ and $275°$. This stack air contained very high concentrations of NO (up to

183   200 ppbv in individual plumes), leading to complete titration of O_3, while H_2O_2 was not affected

184   at all on the short time scales involved, as has been observed previously (Weller et al., 2000). In

185   total 53% of the observations were effected by stack emissions. Therefore we used Ox (O_3 +

186   NO_2) for the experimental data, to deduce the original O_3 concentration that would have occurred

187   without NO-titration to NO_2. In general, the difference between Ox and O_3 is marginal due to the

188   very low NOx mixing ratios of less than 20 pptv in the remote marine boundary layer over the

189 southern Atlantic and less than 200 pptv east of South Africa (Hosaynali Beygi et al., 2011). Thus

190 the error in O_3 using Ox in all cases is smaller than 2 %. From the model only the original O_3 data

191 are used.

192

193 **3.2 Distribution of measured and simulated trace gases**

194 Figure 3 shows the time series for measured and simulated ozone mixing ratios. Observed O_3

195 varies between 17 and 25 ppbv, with lower values in the south-western Atlantic and higher values

196 closer to Africa. The model qualitatively reproduces this gradient with a slight tendency to

197 underestimate O_3 mixing ratios during the first part of the cruise (March 10 – March 14) and a

198 slight overestimation between March 15 and 17. During the last part of the cruise after March 17

199 both model and observations agree quite well. Overall, the mean observed and simulated O_3 are

200 20.3 ± 1.8 ppbv and 19.7 ± 2 ppbv, respectively. A least-square fit between simulated (y-axis)

201 and observed (x-axis) ozone yields a slope of 0.98 ± 0.01 and an offset of -0.43 ± 0.21 ppbv. The

202 regression coefficient R^2 is rather low (0.2). Taking into account that observed Ox measurements

203 are affected by background NO_2, the agreement between observations and model results is quite

204 satisfactorily. Observations and model results are in good agreement with observations by

205 Helmig et al. (2012) during the GasEx 2008 cruise in the southern Atlantic at 50° S between

206 65°W and 35°W in March 2008, who reported an average O_3 mixing ratio of 18.3 ppbv. Similar

207 O_3 mixing ratios of the order of 20 ppbv were also observed over the southern Atlantic, south of

208 40° S, during three Polarstern cruises in November 1990 (Slemr and Tremmel, 1994),

209 October/November 1994 (Junkermann and Stockwell, 1999) and March 1999 (Jacobi and

210 Schrems, 1999). As discussed in Lelieveld et al. (2004) seasonal variations of O_3 in the latitude

211 band between 40° and 60° S are rather small, with slightly lower values in austral summer. For

212 the period between 1977 and 2002 the calculated O_3 trend for this latitude band is 0.17 ± 0.08

213 ppbv/year (Lelieveld et al., 2004), indicating a moderate increase of approximately 1 ppbv

214 between 2002 and 2007. Based on the limited number of observations during OOMPH a

215 conclusion about the continuation of this trend is not possible.

216 Time series of measured and simulated H_2O_2 are shown in Figure 4. During the first part of the

217 cruise (March 10 to 14) observed H_2O_2 mixing ratios indicate small variability at levels between

218 200 and 300 pptv. During this period the model significantly underestimates observed H_2O_2, by

219 more than a factor of two. After March 14 in the eastern part of the South Atlantic H_2O_2 mixing

220 ratios tend to increase both in the observations and the model simulations, with the model

7

221 overestimating observations during the first part, in particular on March 15, while later on

222 measurements and model results agree quite well. A period of relatively high H_2O_2 (in excess of

223 1 ppbv) was observed and simulated after midnight on March 16, southwest of the African coast

224 (see Figure 1). On average observed and simulated H_2O_2 were 350 ± 220 pptv and 310 ± 240

225 pptv, respectively. Slope and intercept of a least-square regression analysis are 2.04 ± 0.04 and -

226 0.27 ± 0.04 ppbv, respectively. The regression coefficient R^2 is 0.46. The imperfect agreement

227 here between model results and observations is due to the rather limited dynamical range of

228 mixing ratios and the strong offset during the first part of the cruise. This is also the case for O_3.

229 As can be deduced from the time series (Figure 4) the model tends to reproduce trace gas levels

230 over the Southern Atlantic. The measured H_2O_2 mixing ratios are comparable to previously

231 reported observations south of 35°S in the Atlantic lower troposphere, being approximately 200 –

232 300 pptv (Slemr and Tremmel, 1994; Junkerman and Stockwell, 1999; Weller et al., 2000).

233 Observations of CH_3OOH mixing ratios are shown in the time series in Figure 5 along with

234 EMAC simulations. The temporal evolution is similar to H_2O_2, with low values (less than 200

235 pptv) during the first part of the cruise, a strong mixing ratio increase starting on midnight of

236 March 16 and lower concentrations afterwards. The relative change is reproduced by the model,

237 with a general tendency to overestimate CH_3OOH mixing ratios except during the period when

238 the high peak was encountered on March 16. Average measured CH_3OOH mixing ratios are 280

239 ± 250 pptv, while the model calculates a mean value of 450 ± 190 pptv. The offset between

240 model and observations is clearly shown in the least-square regression analysis that yields an

241 intercept at 0.18 ± 0.05 ppbv and a slope of 0.37 ± 0.12 at an R^2 of 0.6. In general the observed

242 mixing ratios are in good agreement with reported levels in the literature (Slemr and Tremmel,

243 1994; Junkerman and Stockwell, 1999; Weller et al., 2000).

244 With the exception of the mixing ratio peaks on March 16, the variability of O_3, H_2O_2 and

245 CH_3OOH is small across the South Atlantic basin between South America and South Africa. The

246 slightly northward orientation of the ship track results in a steady increase in temperature and

247 photolysis rates (Hosaynali Beygi et al., 2011) leading to increasing photochemical activity that is

248 likely responsible for the slight increase of the mixing ratios of the three species from the south-

249 western to the north-eastern part of the South Atlantic. As shown in a backward trajectory

250 analysis presented in Hosaynali Beygi et al. (2011) the air mass origin did not change throughout

251 the cruise. All air masses encountered during the cruise originated in the western Antarctic

8

252 Peninsula during the preceding week and had not been in contact with land surfaces for at least 5
253 days.

254 **3.3 Discussion**

255 Based on H_2O_2 mixing ratios and the comparison between observations and model results, one
256 can differentiate three different periods in Fig. 4: From March 10 to 14 the model significantly
257 underestimates the H_2O_2 mixing ratios, while the agreement is much better during the final phase
258 of the campaign (after March 17). In between these two periods H_2O_2 mixing ratios show a strong
259 increase to well above 1 ppbv that is well reproduced by the model.
260 Similar behavior is also observed for ozone (Figure 3). The model also tends to underestimate O_3
261 mixing ratios during the early phase of the campaign, while the agreement is much better in the
262 second half of the campaign. On the other hand, the CH_3OOH mixing ratios are almost always
263 overestimated by the model (Figure 5). Considering the ratio between CH_3OOH and H_2O_2 there
264 is an even stronger discrepancy (Figure 6). Over the whole campaign, the observed ratio varies
265 between 0.5 and 1with a mean value and standard deviation of 0.8 ± 1.1, while the model predicts
266 a time dependent ratio between 2 and 4 during the first half of the campaign and lower values, in
267 good agreement with the observations, during the second half of the campaign. Hence one
268 problem seems to be that the model underestimates H_2O_2 during the early phase of the campaign,
269 due to either an underestimation of the H_2O_2 production or an overestimation of the sinks. Gas
270 phase H_2O_2 in the marine boundary layers stems from the recombination of two HO_2 radicals. As
271 shown by Hosaynali Beygi et al. (2011), EMAC reproduces observed HO_2 levels (observations
272 are shown in Figure 10 and model results in Figure 11 of Hosaynali Beygi et al., 2011) during the
273 whole campaign and indicates similar levels for HO_2 and CH_3O_2, the precursors of CH_3OOH. A
274 scatter plot (not shown) and a regression analysis indicate that the model tends to overestimate
275 observed HO_2 by approximately 20 % throughout the campaign (HO_2(obs) = (0.786 ± 0.004) x
276 HO_2(model) – (0.44 ± 0.03); R^2= 0.87). The total uncertainty of the HO_2 measurements is $\pm$ 35 %
277 (2σ) (Hosaynali Beygi et al., 2011), indicating that HO_2 observations and simulations agree
278 within the uncertainties of the observations (a total uncertainty for the simulations is not available
279 and not easy to derive). Thus the simulation tends to overestimate the H_2O_2 source by about 40
280 %, assuming that HO_2 reacts only with HO_2 and reactions with NO are negligible, which is
281 justified by the very low NOx levels of less than 20 pptv in both observations and simulations.
282 Given that the precursor levels are slightly overestimated by EMAC, it is very unlikely that an

283   underestimation of the peroxide production is responsible for the H_2O_2 underestimation during

284   the first half of the campaign. This indicates that the discrepancies are due to an overestimation of

285   the H_2O_2 sinks in the model during this period. Photochemical sinks (reaction with OH and H_2O_2

286   photolysis) are also unlikely causes, since the model also reproduces OH concentrations (Beygi et

287   al., 2011) and radiation intensities (not shown). The model simulations of the photochemical

288   H_2O_2 sinks indicate that during noon the maximum contribution of H_2O_2 photolysis and reaction

289   with OH varies between 2 % (March 11) and a maximum of 12 % (March 19). Hence the

290   influence of the photochemical sinks on the H_2O_2 mixing ratio is marginal (setting both sinks to

291   zero would increase the simulated H_2O_2 mixing ratios by approx. 10 %). Other sinks of H_2O_2, in

292   particular H_2O_2 uptake on aerosols, were not considered in the model simulation and thus cannot

293   be responsible for the underestimation of the H_2O_2 mixing ratio in the simulations. The same is

294   true for HO_2 loss on aerosols, which was also not considered in the model simulation.

295   This leaves physical removal processes, such as rainout and dry deposition to the surface, as most

296   likely causes. Although the model predicts some rain events, they are not particularly extensive

297   during the first phase, when the problems occur. A striking observation is that the wind speeds

298   are significantly higher during the first part of the campaign, being well above 10 m/s up to

299   March 15 (Figure 1), while they are generally lower in the second half of the campaign. The dry

300   deposition in EMAC (Kerkweg et al., 2006) is based on the dry deposition scheme of Ganzeveld

301   et al. (Ganzeveld and Lelieveld, 1995, Ganzeveld et al., 1998) partly following Wesley (1989).

302   For highly soluble species like H_2O_2 the ocean surface resistance is assumed to be negligible and

303   the deposition velocity strongly depends on the wind speed, which determines the transfer

304   velocity to the ocean surface. For less soluble species like O_3 and MHP the dry deposition

305   velocity is dominated by a non-zero ocean uptake resistance (Ganzeveld and Lelieveld, 1995).

306   The deposition velocity calculated by the model for O_3 does not depend on the wind speed and is

307   about 0.05 cm/s, indicating that the deposition loss is limited by the ocean uptake resistance. On

308   the other hand, the H_2O_2 deposition velocity is a strong function of wind speed, linearly

309   increasing from ~ 0.5 cm/s at a wind speed of 5 m/s to about 1.8 cm/s at 10 m/s. This indicates

310   that the deposition loss for this highly soluble species is limited by the transfer velocity to the

311   ocean surface. These values are in good agreement with those derived from airborne

312   measurements in the marine boundary layer over the Atlantic Ocean off the coast of South

313   America during GABRIEL 2005 (Stickler et al., 2007). Based on H_2O_2 observations and an

314   assumed rate of entrainment from the free troposphere Stickler et al. estimated an H_2O_2

10

315   deposition velocity of 1.3 cm/s (range <0.1 to >1.8 cm/s, depending on the assumptions for the

316   entrainment rate) at a wind speed of 6 m/s. The single column model used in the study of Stickler

317   et al. (2007) yielded a maximum deposition velocity of 0.5 cm/s at that wind speed, which is in

318   good agreement with the EMAC results. Accordingly, due to the absence of low clouds and

319   precipitation during the campaign (for the considered period) dry deposition is the dominant loss

320   process for H_2O_2 in the model, even during the day. During the night dry deposition is the only

321   loss mechanism, as photochemical destruction ceases. The model indicates that during daytime

322   the contribution of dry deposition to total H_2O_2 loss varies between 98 % (noon values) during

323   the first part of the campaign (March 11th to 14th) and about 90 % during the second half (after

324   March 15), due to a combination of decreasing dry deposition loss due to decreasing wind speeds

325   and a simultaneous increase by enhanced photochemical activity at lower latitudes. We

326   performed a sensitivity study (SR1) with EMAC, limiting the maximum wind used in the

327   deposition calculation to 5m/s, resulting in a maximum deposition velocity of H_2O_2 of around 0.6

328   cm/s. The green line in Figure 4 shows that this leads to an increase in simulated H_2O_2 mixing

329   ratios by approximately 50 % (mean calculated mixing ratio: 460 ± 350 pptv). It should be

330   mentioned that globally this effect is strongest in the marine boundary layer in regions of high

331   wind speed, notably in the latitude band between 40° and 60° of the storm tracks in both

332   hemispheres. Outside of these regions the effect is much smaller and leads to increases in the

333   H_2O_2 mixing of less than 20%. Thus it appears that the differences between model simulations

334   and H_2O_2 observations are due to a model overestimation of dry deposition to the ocean at high

335   wind speed. This hardly affects CH_3OOH and O_3 whose deposition loss is limited by their

336   solubility and thus independent of wind speed, while H_2O_2 is much more strongly affected. The

337   importance of the deposition parameterization, being a critical process in the simulation of H_2O_2

338   in the lower troposphere was also emphasized by Chang et al. (2004), who performed sensitivity

339   studies with a single column model to simulate observations from PEM-Tropics B.

340   Another interesting feature of the H_2O_2 time series in Fig. 4 is the strong increase of H_2O_2 in the

341   night from March 15 to 16. Shortly before midnight the H_2O_2 mixing ratio increases strongly

342   from ~ 0.7 ppbv up to about 1.5 ppbv, and decreasing to the previous mixing ratios before noon

343   on March 16. The sudden increase occurs together with a similar increase in CH_3OOH (Figure 5),

344   which is well reproduced by EMAC. Since the sudden increase in H_2O_2 and CH_3OOH occurs

345   during nighttime a photochemical source can be excluded. During this phase of the campaign the

346   ship was south of the southern tip of Africa. One explanation for the sudden increase could be a

11

347   change in air mass origin. Heikes et al. (1996) observed a significant increase of marine boundary

348   layer H_2O_2 mixing ratios north of 20°N in continental outflow. Trajectory calculations for the

349   OOMPH campaign were presented in the supplements to the paper by Hosaynali Beygi et al.

350   (2011). They indicate, however, no change in air mass origin during the period between March

351   15 and 17, so that this option can be dismissed.

352   Due to the dry deposition close to the ocean surface, both H_2O_2 and CH_3OOH are expected to

353   exhibit an increase in mixing ratios with height. Aircraft observations over the ocean indeed show

354   maxima of both species above the marine boundary layer (Heikes et al., 1996; O'Sullivan et al.,

355   1999; O'Sullivan et al., 2004; Stickler et al., 2007). Thus transport from above the boundary layer

356   can be a source of H_2O_2 and CH_3OOH for the marine boundary layer. Observations of the

357   boundary layer height were not made during the OOMPH campaign, thus we have to rely on

358   model results. The curtain plot in Figure 7 shows a time series of the vertical profiles for O_3

359   (upper panel) and H_2O_2 (lower panel). Superimposed is the temporal evolution of the boundary

360   layer height calculated by EMAC. Note that the diurnal variation of the boundary layer height

361   during March 17th – 19th is related to the proximity to the African continent. Due to the limited

362   resolution of the model the data points here are interpolated between an oceanic and a continental

363   grid cell, leading to a diurnal evolution of the boundary layer height that resembles that of a

364   continental boundary layer instead of the marine boundary layer. Shortly before the event the

365   simulation indicates a very shallow boundary layer (~ 200 m), that starts to increase around

366   midnight on March 16th. Hence the increase in H_2O_2 is related to an increase in boundary layer

367   height, and downward mixing of air masses that have not been affected by deposition and thus

368   having higher mixing ratios of peroxides. Thus it seems that nighttime transport of free

369   tropospheric air into the marine boundary layer is responsible for the concentration increase

370   during the period from March 15th to 16th. This vertical redistribution process should also affect

371   other species with a positive altitude gradient, in particular ozone. Model profiles indicate that the

372   mixing ratio gradient for O_3 is much smaller than for H_2O_2 (upper panel in Fig. 7). This is

373   consistent with the moderate change in O_3 mixing ratios during this event.

374   Finally, the difference in simulated and observed absolute mixing ratios of CH_3OOH needs to be

375   addressed. Figure 5 indicates that although the model reproduces the relative changes quite well,

376   the absolute values are off by a factor of about 2, with the model being consistently higher. The

377   relative difference is higher in the beginning and lower towards the end of the campaign, but the

378   absolute difference remains about 200 pptv. There are several potential explanations for this

12

379   discrepancy. First, as mentioned in section 2.2 CH_3OOH was not directly measured, but inferred

380   from the ROOH signal, assuming that CH_3OOH is the only organic hydroperoxide and that the

381   sampling efficiency can be calculated according to Lee et al. (2000). An experimental verification

382   of the sampling efficiency was not performed (contrary to H_2O_2) since no CH_3OOH gas phase

383   source was available. If the actual sampling efficiency was lower than the calculated 60%, this

384   could close the gap between observations and model results. Additionally, the sampling

385   efficiency would have to be lower at the beginning of the campaign and higher later on, since a

386   simple multiplication by a factor cannot account for the rather constant absolute difference over

387   the campaign. Therefore, although an error in the sampling efficiency cannot be excluded, it is

388   unlikely the only source of the discrepancy between model and observations.

389   As discussed above, Hosaynali Beygi et al. (2011) demonstrated that EMAC very well

390   reproduces the HO_2 measurements made during the OOMPH cruise. Since the precursor for H_2O_2

391   is simulated correctly by the model, one can assume that the source strength for H_2O_2 is correctly

392   simulated. The model predicts CH_3O_2 concentrations that are similar to HO_2, but unfortunately

393   measurements of CH_3O_2 were not made. Thus it is not possible to validate the model predicted

394   precursor concentrations for CH_3OOH. But as discussed in Hosaynali Beygi et al. (2011) the

395   simulated CH_3O_2 levels are quite realistic. Recently Fittschen et al. (2014) posed that the reaction

396   of CH_3O_2 with OH radicals at low NOx concentrations can be a significant sink of methylperoxy

397   radicals and thus could reduce CH_3OOH formation. In a sensitivity study (SR2) this reaction was

398   included in the chemistry code of EMAC (Bossolasco et al., 2014). Additionally, we considered

399   that in addition to CH_3OOH the reaction of CH_3O_2 with HO_2 also produces HCHO to some

400   extend (Ayers et al., 1997). The green line in Figure 6 indicates that including these additional

401   reaction pathways reduces the mixing ratio of CH_3O_2 in the marine boundary layer of the South

402   Atlantic by about 30%, yielding an average mixing ratio of 300 ± 110 pptv compared to the

403   observed 180 ± 50 pptv. It seems that the missing reaction between CH_3O_2 and OH is responsible

404   for a largest part of the CH_3OOH overestimation by the model, in particular during the second

405   half of the cruise when OH concentrations are high. In general, the contribution of this reaction

406   increases with increasing OH concentration, which leads globally to a maximum impact in the

407   tropical lower troposphere over the Pacific and Indian Oceans. The contribution of the HCHO

408   channel in the reaction of CH_3O_2 with HO_2 is rather constant with a branching ratio of about

409   10%. Nevertheless, due to the uncertainties in both measurements and modeling the explanation

410   for the difference in CH_3OOH simulation vs. observations remains ambiguous.

411   By combining both the reduced H_2O_2 deposition velocity and the reduced CH_3OOH source due to

412   the competing reaction of CH_3O_2 with OH in an additional sensitivity simulation (SR3) the

413   simulated CH_3OOH/H_2O_2 ratio is reduced to a mean value of 1.01 ± 1.06 (green line in Figure 6),

414   much closer to the observed value (0.8 ± 1.1).

415   Note that an underestimation of entrainment from the free troposphere would also explain the

416   underestimation of the H_2O_2 (and O_3) mixing ratios during the first phase of the campaign.

417   However, this leads to an inconsistency with the MHP data, which would be affected by the same

418   transport. Similar to H_2O_2 and O_3, MHP mixing ratios increase with altitude and show a

419   maximum above the boundary layer (Stickler et al., 2007, Klippel et al. 2011). Thus one would

420   expect that a transport limitation from the free troposphere in the simulations would also produce

421   an underestimation of the simulated MHP concentrations in the MBL, but the opposite is the

422   case; actually the model significantly overestimates MHP. Therefore, we conclude that different

423   processes are responsible for the temporal underestimation of H_2O_2 (during the first part of the

424   campaign) and the time independent overestimation of MHP, as most clearly corroborated in the

425   time series of the ratio of these two species in Figure 6.

426   **Summary and conclusions**

427   Hydrogen peroxide, MHP and ozone have been measured in the marine boundary layer over the

428   South Atlantic Ocean during the austral summer in 2007. Observed mixing ratios are consistent

429   with values reported in the literature. Simulations with the atmospheric chemistry model EMAC

430   indicate that it qualitatively reproduces the observations very well. It also captures the downward

431   mixing of high concentrations of H_2O_2 and CH_3OOH during a nighttime increase in boundary

432   layer height south of the African continent. Quantitatively, the model tends to underestimate

433   H_2O_2 mixing ratios during the first part of the cruise. During this part we experienced very high

434   wind speeds, in excess of 15 m/s. Later on during the cruise much lower wind speeds were

435   encountered for which the model accurately reproduces observed H_2O_2 mixing ratios. A similar

436   tendency has been observed for ozone. The most likely reason for the discrepancy is that the

437   model parameterization of trace gas deposition to the ocean surface tends to overestimate the dry

438   deposition loss of the soluble and reactive H_2O_2 at high wind speeds. This was confirmed by a

439   model sensitivity study with limited (at 5 cm/s) deposition velocity. MHP, which is less soluble

440   and reactive, is not as much of affected by dry deposition, although EMAC significantly

441   overestimates its mixing ratio. This overestimation is rather constant over the campaign and

14

442   indicates an offset of approximately 200 pptv. The reasons for this discrepancy are not easy to

443   identify, since the measurements provide less stringent constraints than for H_2O_2. MHP was

444   estimated from a total ROOH signal, assuming MHP being the only ROOH component and a

445   sampling efficiency of 60 % compared to H_2O_2. Fittschen et al. (2014) recently suggested that a

446   competing reaction of the CH_3O_2 radicals with OH can significantly diminish the source of MHP

447   in the marine boundary layer, in particular at the low NOx concentrations observed during

448   OOMPH. A sensitivity study with EMAC indicates that this reaction reduces the CH_3O_2 mixing

449   ratio by about 30 %, increasing with decreasing latitude due to the meridional gradient in OH

450   radical concentrations. Although this is a significant change, bringing CH_3OOH closer to

451   observations, it appears to be insufficient to fully remove the discrepancy between simulated and

452   observed CH_3OOH mixing ratios during OOMPH.

457

458

459

References

Ayers, G.P., Gillet, R.W., Granek, H., de Serves, C., and Cox, R.A.: Formaldehyde production in clean marine air, Geophys. Res. Lett., 24, 401-404, 1997.

Bossolasco, A., Farago, E.P., Schoemacker, C., and Fittschen, C.: Rate constant of the reaction between CH_3O_2 and OH radicals, Chem. Phys. Lett., 593, 7-13, 2014.

Chang, W., Lee, M., and Heikes, B.G.: One-dimensional photochemical study of H_2O_2, CH_3OOH, and HCHO in the marine boundary layer during Pacific Exploratory Mission in the Tropics (PEM-Tropics) B, J. Geophys. Res., 109, D06307, doi:10.1029/2003JD004256, 2004.

Fittschen, Ch., Whalley, L.K., and Heard, D.E.: The raction of CH_3O_2 radicals with OH radicals: A neglected sink in the remote atmosphere, Environm. Sci. & Technol., 48, 7700-7701, doi:10.1021/es502481q, 2014.

Ganzeveld, L., and J. Lelieveld, J.: Dry deposition parameterization in a chemistry general circulation model and its influence on the distribution of reactive trace gases, J. Geophys. Res., 100, 20,999-21,012, 1995.

Ganzeveld, L., Lelieveld, J., and Roelofs, G.-J.: Dry deposition parameterization of sulfur oxides in a chemistry and general circulation model, J. Geophys. Res., 103, 5679-5694, 1998.

Heikes, B.G., Lee, M., Bradshaw, J., Sandholm, S., Davis, D.D., Crawford, J., Rodriguez, J., Liu, S., McKeen, S., Thornton, D., Bandy, A., Gregory, G., Talbot, R., and Blake, D.: Hydrogen peroxide and methylhydrogenperoxide distributions related to ozone and odd hydrogen over the North Pacific in the fall of 1991, J. Geophys. Res., 101, 1891-1905, 1996.

Helmig, D., Lang, E.K., Bariteau, L., Boylan, P., Fairall, C.W., Ganzeveld, L., Hare, J.E., Hueber, J., and Pallandt, M.: Atmophere-ocean ozone fluxes during the TexAQS 2006, STRATUS 2006, GOMECC 2007, GasEx 2008 and AMMA 2008 crusies, J. Geophys. Res., 117, D04305, doi:10.1029/2011JD015955, 2012.

Hosaynali Beygi, Z., Fischer, H., Harder, H.D., Martinez, M., Sander, R., Williams, J., Brookes, D.M., Monks, P.S., and Lelieveld, J.: Oxidation photochemistry in the Southern Atlantic boundary layer: unexpected deviations of photochemical state, Atmos. Chem. Phys., 11, 8497-8513, doi:10.5194/acp-11-8497-2011, 2011.

Jacobi, H.-W., and Schrems, O.: Peroxyacetyl nitrate (PAN) distribution over the South Atlantic Ocean, Phys. Chem. Chem. Phys., 1, 5517-5521, 1999.

Jöckel, P., Sander, R., Kerkweg, A. Tost, H., and Lelieveld, J.: Technical note: The Modular Earth Submodel System (MESSy) – a new approach towards earth system modelling, Atmos. Chem. Phys., 5, 433-444. doi:10.5194/acp-5-433-2005, 2005.

493   Jöckel, P., Tost, H., Pozzer, A., Brühl, C. Buchholz, J., Ganzeveld, L., Hoor, P., Kerkweg, A.,
494   Lawrence, M.G., Sander, R., Steil, B., Stiller, G., Tanarthe, M., Taraborrelli, D., van Aardenne,
495   J., and Lelieveld, J.: The atmospheric chemistry general circulation model ECHAM5/MESSy1:
496   consistent simulation of ozone from the surface to the mesosphere, Atmos. Chem. Phys., 6, 5067-
497   5104, doi:10.5194/acp-6-5067, 2006.

498   Jöckel, P., Kerkweg, A., Pozzer, A., Sander, R., Tost, H., Riede, H., Baumgaertner, A., Gromov,
499   S., and Kern, B.: Development cycle 2 of the Modular Earth Submodel System (Messy 2),
500   Geoscientific Model Development, 3, 717-752, doi:10.5194/gmd-3-717-2010, 2010.

501   Junkerman, W. and Stockwell, W.: On the budget of photooxidants in the marine boundary layer
502   of the tropical South Atlantic, J. Geophys. Res., 104, 8039-8046, 1999.

503   Kerkweg, A., Buchholz, J. Ganzeveld, L., Pozzer, A., Tost H., and Jöckel, P.: Technical note: An
504   implementation of the dry removal process DRY DEPosition and SEDImentation in the Modular
505   Earth Submodel System (MESSy), Atmos. Chem. Phys., 6, 4617-4632, doi:10.5194/acp-6-4617-
506   2006, 2006a.

507   Kerkweg, A., Sander, R., Tost, H., and Jöckel, P.,: Technical note: Implementation of prescribed
508   (OFFLEM), calculated (ONLEM), and pseudo-emissions (TNUDGE) of chemical species in the
509   Modular Earth Submodel System (MESSy), Atmos. Chem. Phys., 6, 3603-3609,
510   doi:10.5194/acp-6-3603-2006, 2006b.

511   Lelieveld, J., van Aardenne, J., Fischer, H., de Reus, M., Williams, J., and Winkler, P.: Increasing
512   ozone over the Atlantic Ocean, Science, 304, 1483-1487, 2004.

513   Levy, H. II: Normal Atmosphere: Large radical and formaldehyde concentrations predicted,
514   Science, 173, 141-143, 1971.

515   Kieber, R.J., Cooper, W.J., Willey, J.D., and Avery Jr., G.B.: Hydrogen peroxide at the Bermuda
516   Atlantic Time Series Station. Part 1: Temporal variability of atmospheric hydrogen peroxide and
517   its influence on seawater concentrations, J. Atmos. Chem., 39, 1-13, 2001.

518   Klippel, T., Fischer, H., Bozem, H., Lawrence, M.G., Butler, T., Jöckel, P., Tost, H., Martinez,
519   M., Harder, H., Regelin, E., Sander, R., Schiller, C.L., Stickler, A., and Lelieveld, J.: Distribution
520   of hydrogen peroxide and formaldehyde over central Europe during the HOOVER project,
521   Atmos. Chem. Phys., 11, 4391-4410, doi:10.5194/acp-11-4391-2011, 2011.

522   Lazarus, A.L., Kok, G.L., Gitlin, S.N., and Lind, J.A.: Automated fluorometric method for
523   hydrogen peroxide in atmospheric precipitation, Anal. Chem., 57, 917-922, 1985.

524   Lazarus, A.L., Kok, G.L., Lind, J.A., Gitlin, S.N., Heikes, B.G., and Shetter, R.E.: Automated
525   fluorometric method for hydrogen peroxide in air, Anal. Chem., 58, 594-597, 1986.

526 Lee, M., Heikes, B.G., and O'Sullivan, D.W.: Hydrogen peroxide and organic peroxide in the
527 troposphere: a review, Atmos. Environm., 34, 3475-3494, 2000.

528 O'Sullivan, D.W., Heikes, B.G., Lee, M., Chang, W., Gregory, G.L., Blake, D.R., and Sachse,
529 G.W.: Distribution of hydrogen peroxide and methylhydroperoxide over the Pacific and South
530 Atlantic Oceans, J. Geophys. Res., 104, 5635-5646, 1999.

531 O'Sullivan, D.W., Heikes, B.G., Snow, J., Burrow, P., Avery, M., Blake, D.R., Sachse, G.W.,
532 Talbot R.W., Thornton, D.C., and Bandy, A.R.: Long-term and seasonal variations in the levels
533 of hydrogen peroxide, methylhydroperoxide, and selected compounds over the Pacific Ocean, J.
534 Geophys. Res., 109, D15S13, doi:10.1029/2003JD003689, 2004.

535 Sander, R., Kerkweg, A., Jöckel, P., and Lelieveld, J.: Technical note: The new comprehensive
536 atmospheric chemistry module MECCA, Atmos. Chem. Phys., 5, 445-450, doi:10.5194/acp-5-
537 445-2005, 2005.

538 Slemr, F. and Tremmel, H.G.: Hydroperoxides in the marine troposphere over the Atlantic
539 Ocean, J. Atmos. Chem., 19, 371-404, 1994.

540 Stickler, A., Fischer, H., Bozem, H., Gurk, C., Schiller, C., Martinez-Harder, M., Kubistin, D.,
541 Harder H., Williams, J., Eerdekens, G., Yassaa, N., Ganzeveld, L., Sander, R., and Lelieveld, J.,:
542 Chemistry, transport and dry deposition of trace gases in the boundary layer over the tropical
543 Atlantic Ocean and the Guyanas during the GABRIEL field campaign, Atmos. Chem. Phys., 7,
544 3933-3956, doi:10.5194/acp-5-3933-2007, 2007.

545 Thompson, A.M.: The oxidizing capacity of the Earth's atmosphere: Probable past and future
546 changes, Science, 256, 1157-1165, 1992.

547 Tost, H., Jöckel, P., Kerkweg, A., Sander, R., and Lelieveld, J.: Technical note: A new
548 comprehensive SCAVenging submodel for global atmospheric modeling, Atmos. Chem. Phys., 6,
549 565-574, doi:10.5194/acp-6-565-2006, 2006.

550 Weller, R., Schrems, O., Boddenberg, A., Gäb, S., and Gautrois, M.: Meridional distribution of
551 hydroperoxides and formaldehyde in the marine boundary layer of the Atlantic (48°N-35°S)
552 measured during the Albatross campaign, J. Geophys. Res., 105, 14401-14412, 2000.

553 Wesley, M.L.: Parameterization of surface resistances to gaseous dry deposition in regional-scale
554 numerical models, Atmos. Environm., 6, 1293-1304, 1989.

555

556

557   Figure captions:

558

559   Figure 1: Ship track of the Marion Dufresne over the southern Atlantic. The track is color coded
560   with time.

561

562   Figure 2: Time series of observed and simulated temperature and wind speed.

563

564   Figure 3: Time series of observed (red) and simulated (blue) ozone mixing ratios.

565

566   Figure 4: Time series of observed (red) and simulated (blue) hydrogen peroxide mixing ratios. In
567   green a sensitivity simulation (SR 1) of the model is shown with reduced dry deposition velocity
568   (see text for details).

569

570   Figure 5: Time series of observed (red) and simulated (blue) methyl hydroperoxide mixing ratios.
571   The green line shows a sensitivity simulation (SR2) including the reaction of CH_3O_2 with OH
572   (see text for details).

573

574   Figure 6: Simulated (blue) and observed (red) CH_3OOH to H_2O_2 ratio. The green line shows a
575   sensitivity simulation (SR3) including reduced H_2O_2 dry deposition velocity and the reaction of
576   CH_3O_2 with OH (see text for details).

577

578   Figure 7: EMAC simulation of O_3 (top) and H_2O_2 (bottom) vertical profiles versus time.
579   Superimposed is the height of the planetary boundary layer. The increase in boundary layer
580   height in the night from March 15 to 16 is associated with an increase in peroxide mixing ratios.
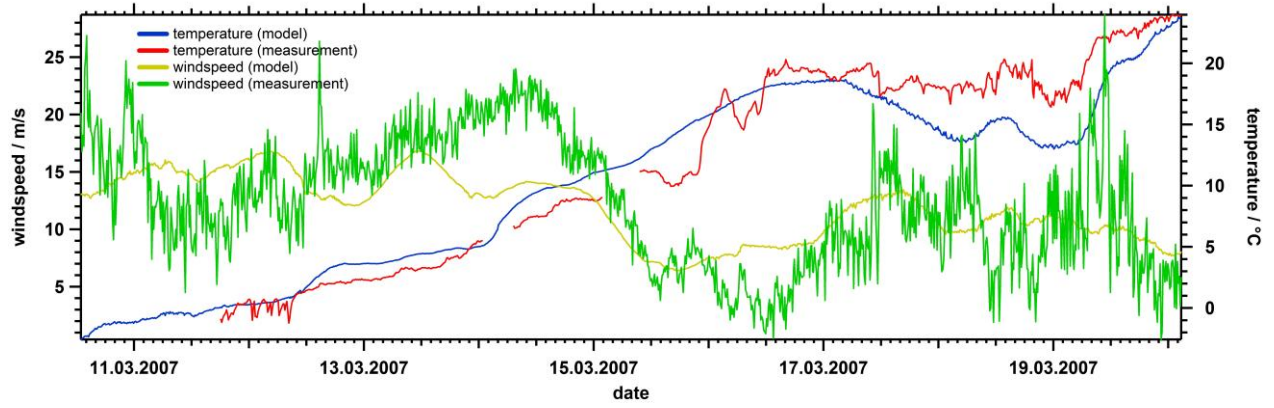
581

582

583

584
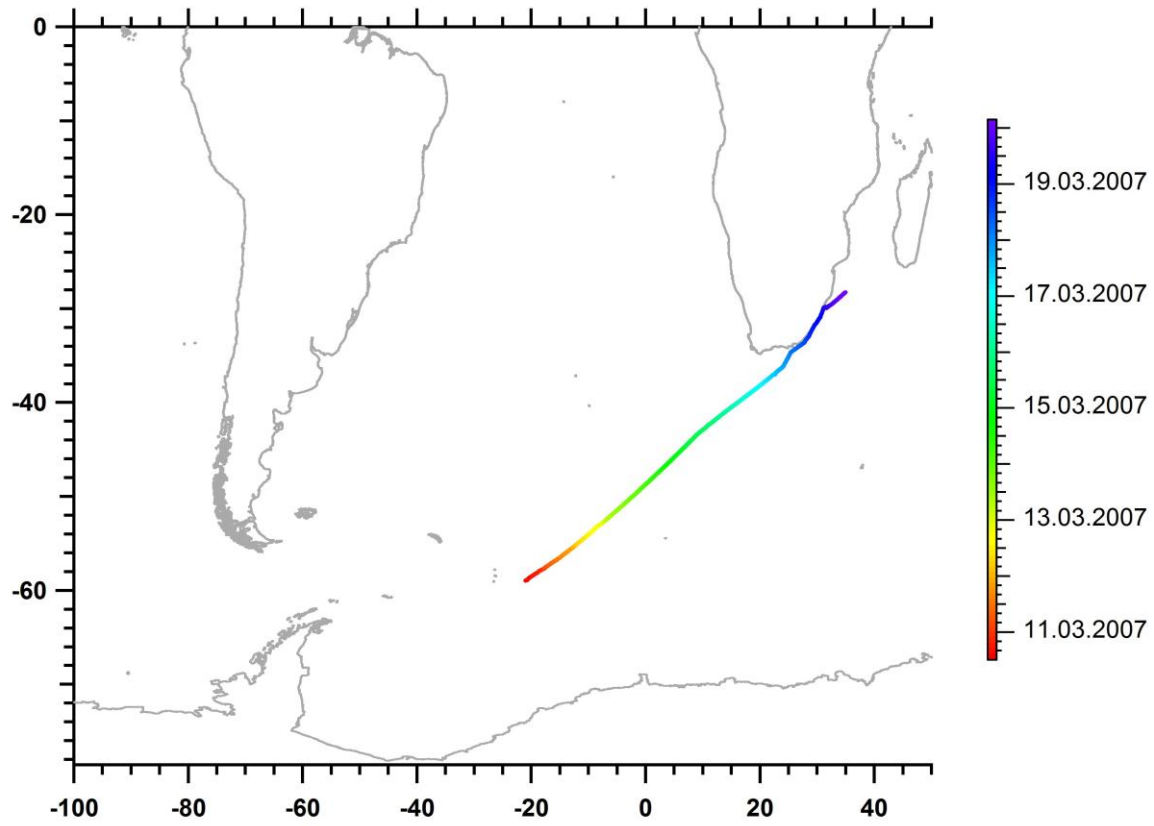
585

586

Figure 1: Ship track of the Marion Dufresne over the southern Atlantic. The track is color coded
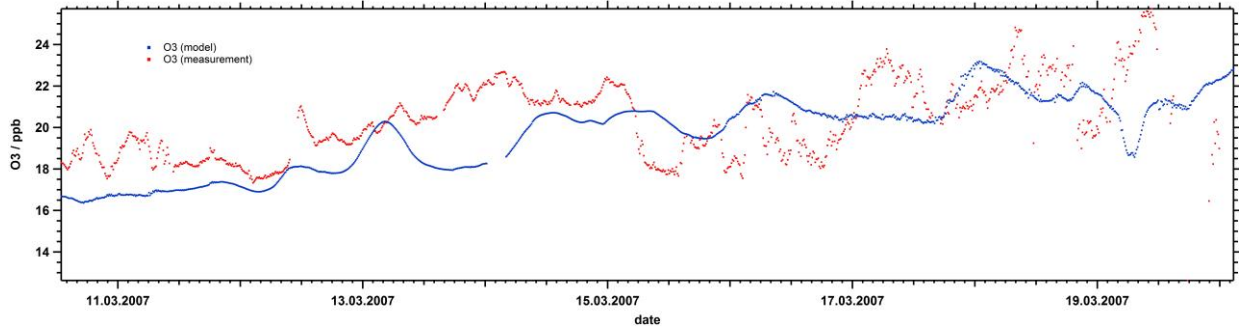with time.

589

590

591   Figure 2: Time series of observed and simulated temperature and wind speed.
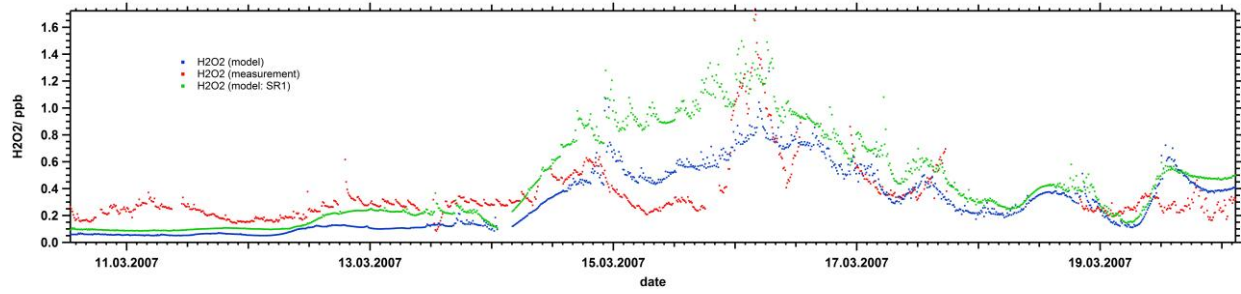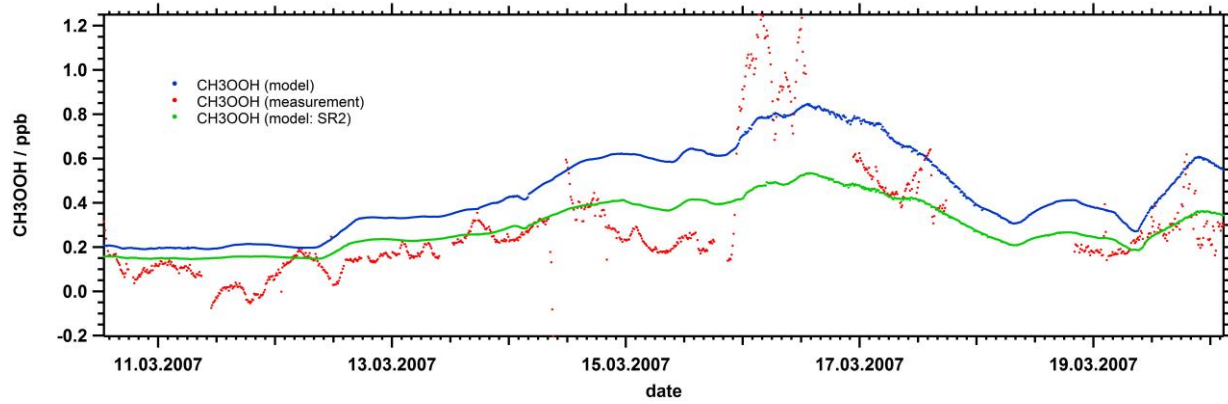
592

593

594   Figure 3: Time series of observed (red) and simulated (blue) ozone mixing ratios.
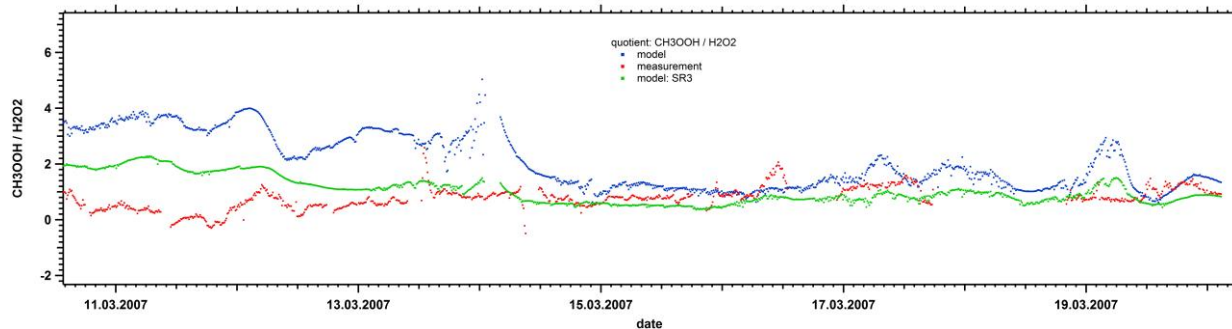
595

596

597 Figure 4: Time series of observed (red) and simulated (blue) hydrogen peroxide mixing ratios. In

598 green a sensitivity simulation (SR 1) of the model is shown with reduced dry deposition velocity
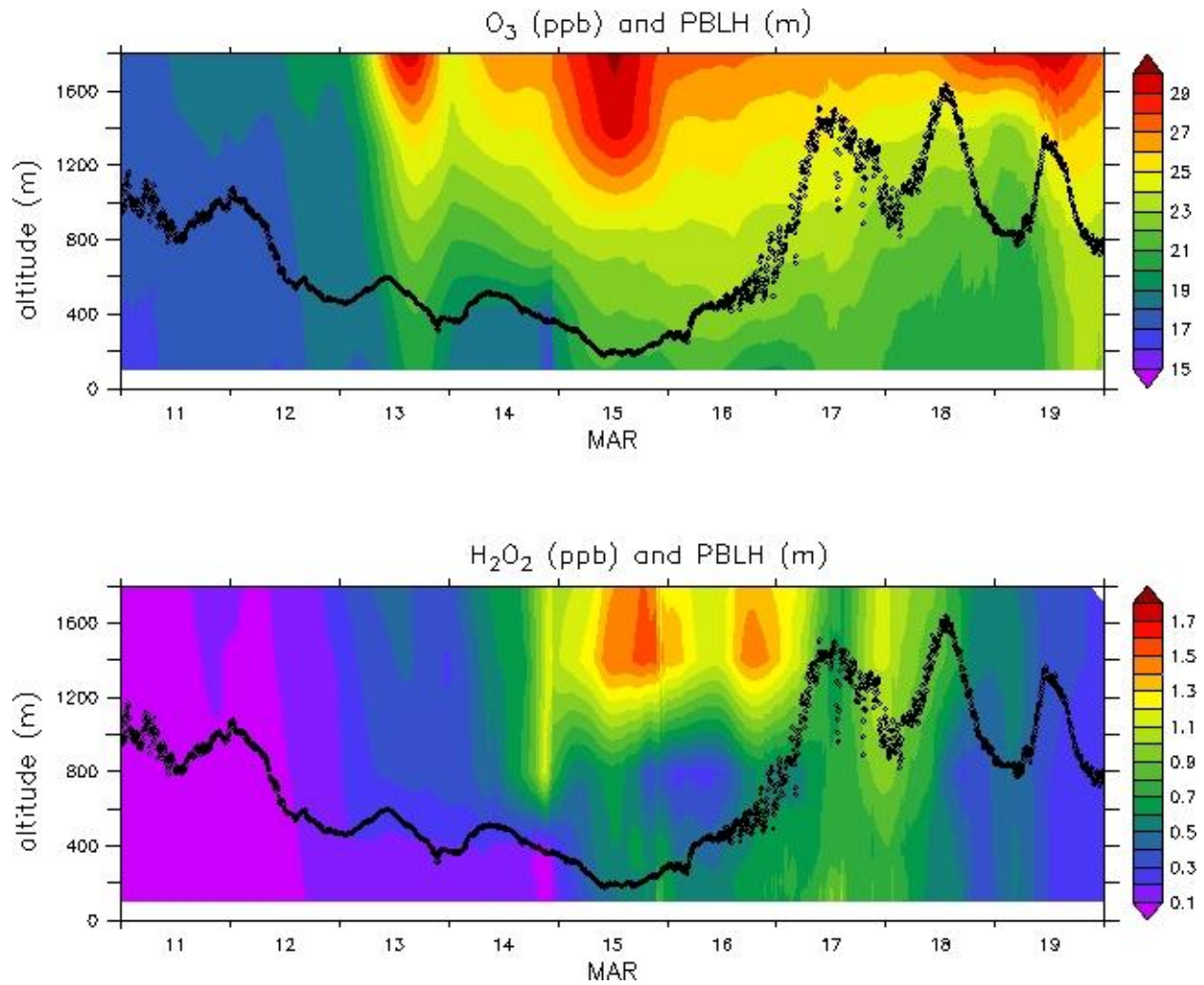
599 (see text for details).

600

601

602   Figure 5: Time series of observed (red) and simulated (blue) methyl hydroperoxide mixing ratios.

603   The green line shows a sensitivity simulation (SR2) including the reaction of CH_3O_2 with OH

604   (see text for details).

605

Figure 6: Simulated (blue) and observed (red) CH_3OOH to H_2O_2 ratio. The green line shows a sensitivity simulation (SR3) including reduced H_2O_2 dry deposition velocity and the reaction of CH_3O_2 with OH (see text for details).

Figure 7: EMAC simulation of O_3 (top) and H_2O_2 (bottom) vertical profiles versus time. Superimposed is the height of the planetary boundary layer. The increase in boundary layer height in the night from March 15 to 16 is associated with an increase in peroxide mixing ratios.